Journal of The Electrochemical Society, **155** (7) A488-A493 (2008)
0013-4651/2008/155(7)/A488/6/$23.00 © The Electrochemical Society

Electrochemical Characterization of Vanadium Oxide Nanostructured Electrode

Elsa A. Olivetti, Kenneth C. Avery, Ikuo Taniguchi, Donald R. Sadoway,* and Anne M. Mayes[z]

Department of Materials Science and Engineering, Massachusetts Institute of Technology, Cambridge, Massachusetts 02139-4307, USA

Films consisting of a vanadium pentoxide (i.e., V_2O_5) phase formed within a rubbery block copolymer were developed for their potential use as nanocomposite cathodes in lithium rechargeable batteries. Films were prepared by sol-gel synthesis from vanadyl triisopropoxide precursor in poly(oligooxyethylene methacrylate)-*block*-poly(butyl methacrylate), incorporating $LiCF_3SO_3$ and carbon black as conductivity additives. The morphology of the films was examined using electron microscopy, and their electrochemical performance was assessed by galvanostatic cycling. An all-solid-state battery comprising a polymer-based cathode and a block copolymer electrolyte was cycled repeatedly. The capacity was measured to be 40 mAh/g and found to be limited by the conductivity of the polymer electrolyte. A comparison between a nanocomposite cathode and a control cathode with the same carbon:vanadium oxide ratio demonstrated higher rate capability for the nanocomposite sample when paired with a liquid electrolyte. This study demonstrates the potential utility of block copolymers in the fabrication of high-surface-area cathodes for lithium batteries.
 [DOI: 10.1149/1.2909560]

Manuscript submitted December 19, 2007; revised manuscript received March 25, 2008. Available electronically May 2, 2008.

Vanadium oxide has been studied extensively as an insertion cathode material for lithium-ion batteries due to its stability, relative safety, low cost, ease of synthesis, and high energy density.[1] Vanadium oxides synthesized via sol-gel chemistry from vanadic acid or vanadyl alkoxides result in amorphous xerogels.[2] One method employed to improve the capacity of sol-gel vanadium oxides in lithium batteries has been altering the way the solvent phase is removed through techniques including supercritical drying,[3] freeze-drying,[4] or solvent exchange.[5,6] The resulting microstructures (called aerogels in the case of supercritical or freeze-drying and ambigels in the case of solvent exchange methods) lead to a higher capacity and rate capability than vanadium oxide xerogels due to increased surface area ($\sim$200 to 400 m^2/g compared to $\sim$20 m^2/g) and reduced diffusion distances for intercalated ions.[7] When cycled between 4.0 and 1.5 V, vanadium oxide aerogels achieved capacities of 410 mAh/g at C/40.[6] Baudrin et al. have used the vanadium oxide aerogel structure to access a metastable phase with capacities in excess of 500 mAh/g.[8] Recently, vanadium oxide sol coated onto colloidal-crystal-templated porous carbon resulted in cathodes with capacities as high as 90 mAh per gram of V_2O_5/carbon composite at specific currents as high as 5 A/g.[9]

Other nanoscale microstructures of vanadium oxide investigated for battery applications include nanoparticles, -tubes, -rolls, -rods, and -ribbons.[10-18] Singhal et al. observed increased capacity for electrodes incorporating partially crystalline nanoparticles (vs coarse-grained particles) of vanadium oxide produced using a combustion-flame/chemical-vapor-condensation process.[10] Patrissi and Martin,[11,12] Sides et al.,[13] and Sides and Martin[16] synthesized vanadium oxide nanorods using track-etched polycarbonate or anodic alumina membranes as templates and demonstrated their increased rate capability and capacity compared to that of thin-film controls. In one study, nanorod arrays exhibited three times the capacity of thin films at discharge rates of 200 C.[11] More recently, Cui et al. demonstrated fully reversible cycling of nanoribbons between $Li_3V_2O_5$ and V_2O_5 phases, which they attributed to rapid phase transformation kinetics in these nanoscale materials.[15] Vanadium oxide nanotubes for battery applications have also been synthesized through hydrothermal methods employing V_2O_5 precursors and structure-directing amphiphiles,[17] and through template-based electrodeposition techniques.[14,18]

In the present work, an alternate synthesis approach is taken to access high surface area-to-volume ratios using microphase-separating block copolymers to structure direct the sol-gel synthesis of vanadium oxide. Our previous research employed the block copolymer electrolyte poly(oligooxyethylene methacrylate)-*block*-poly(n-butyl methacrylate), POEM-*b*-PBMA, as a matrix to grow vanadium oxide within the lithium ion-conducting POEM domains.[19] The present study extends this work by incorporating carbon black (CB) into the nanocomposite films as a conductivity additive, essential for the construction of batteries. The morphology of the films was examined by electron microscopy, and their electrochemical performance was assessed by galvanostatic cycling. The nanocomposite cycled reversibly as a cathode vs lithium using a solid polymer electrolyte and showed improved rate capability over the composite cathode control.

Experimental

The block copolymer POEM-*b*-PBMA was synthesized by atom transfer radical polymerization as described previously.[19,20] The chemical structure of the final POEM-*b*-PBMA block copolymer is shown in Fig. 1. The resulting material comprised 70:30 (wt:wt)

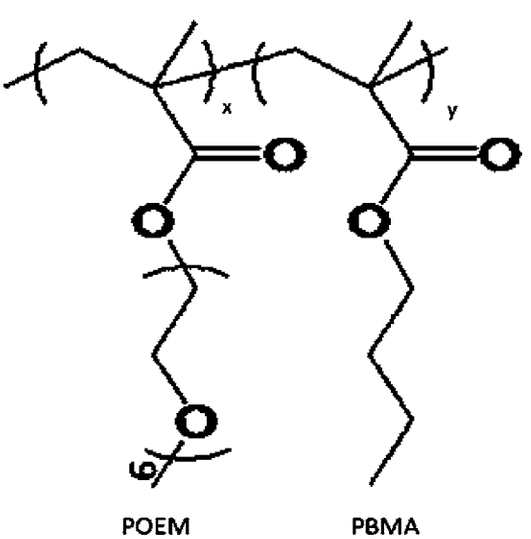

Figure 1. Chemical structure of POEM-*b*-PBMA block copolymer (x = 150, y = 350).

* Electrochemical Society Active Member.
[z] E-mail: amayes@mit.edu

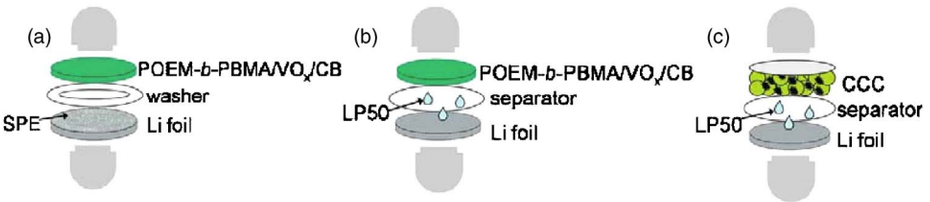

Figure 2. (Color online) Schematic illustrations of test cells. SPE: solid polymer electrolyte, LP50: liquid electrolyte, CCC: conventional composite cathode.

POEM:PBMA and had a molecular weight of 70 kg/mol based on gel permeation chromatography analysis with polystyrene standards. To obtain samples for pyrolysis and scanning electron microscopy (SEM) analysis, coassembled nanocomposite films of POEM-*b*-PBMA incorporating 34 wt % vanadium oxide, termed herein POEM-*b*-PBMA/VO_x, were prepared as previously reported.[19,20] Briefly, POEM-*b*-PBMA (5 wt %) was dissolved in acetone followed by the addition of 50 wt % vanadyl triisopropoxide, $VO(OC_3H_7)_3$ [$VO(O^iPr)_3$,Gelest], and the resulting solution stirred for 30 min. Deionized (DI) water was then added in a molar ratio of 40:1 H_2O:V to initiate gelation. After 1 h stirring, solutions were solvent cast into Teflon dishes (VWR Scientific) and dried in air under glass Petri dishes for >48 h, then heated under vacuum at 80°C overnight to remove residual solvent. Some films were subsequently heated to 400°C under argon (ramped at 3 K/min; held 1.5 h at temperature) to pyrolyze the polymer phase, followed by a heating phase in air (ramped to 400°C at 2 K/min and removed immediately upon reaching temperature) to ensure the formation of V_2O_5. SEM was performed on films after pyrolysis to visualize the morphology of the oxide component. Samples were coated with Au/Pd and mounted with carbon tape onto aluminum posts and the microscopy was performed on a JEOL 6320FV field-emission high-resolution SEM at 1 kV. The surface area of the samples was also determined using the Brunauer, Emmet, and Teller (BET) technique on a Micrometrics ASAP2020 instrument. Prior to the measurement, the samples underwent degassing for 2 h under flowing nitrogen at 100°C. Control films of sol-gel derived VO_x synthesized in the absence of POEM-*b*-PBMA were also characterized.

In order to obtain films that could be cycled as cathodes in Li batteries, modifications were made to the previously described procedure. Lithium trifluoromethanesulfate, $LiCF_3SO_3$ (VWR Scientific), was added to 0.1 g of POEM-*b*-PBMA in the ratio 20:1 EO:Li in the glove box under inert conditions. The polymer/salt mixture was then dissolved in 5 g acetone outside the glove box. After stirring, 0.1 g $VO(O^iPr)_3$ was added to this solution. Films also contained 5 wt % acidified CB (Super P, Cabot Corp.) acting as a conductivity additive. To modify the surface chemistry of the CB, the powder was refluxed with fuming sulfuric acid (VWR Scientific) for 1 h at 80°C.[21] After rinsing with DI water, the CB was dried under vacuum overnight at 100°C, cryoground in liquid nitrogen to break up aggregates, and sonicated in acetone (5 mL) for 1 h. This mixture was added to the precursor/polymer solution.

The mixture containing POEM-*b*-PBMA, $VO(O^iPr)_3$, and CB was allowed to stir for 15 minutes. DI water was subsequently added and the solution cast into a Teflon dish and dried overnight as described above. The resulting 100 μm thick films, termed herein POEM-*b*-PBMA/VO_x/CB, were vacuum dried at 80°C overnight. Thermogravimetric analysis [(TGA), model Q50, TA Instruments, Inc.] was performed on the product film under a nitrogen atmosphere using a heating rate of 20°C/min and a temperature range of 30–600°C. TGA revealed the vanadium oxide content of the final film to be 34 wt % accounting for the presence of the CB component.[19]

Microstructural characterization of the POEM-*b*-PBMA/VO_x/CB films was carried out using a JEOL 2010 CX transmission electron microscope (TEM) in bright field mode at 200 keV. The samples were prepared by cryomicrotoming ~50 nm sections using a diamond knife, placing the sections on copper grids and coating them with ~15 nm of carbon through thermal evaporation. Wide-angle X-ray scattering (WAXS) experiments were carried out on a Rigaku Rotaflex 18 kW rotating anode X-ray generator with Cu Kα radiation operated at 60 kV and 300 mA. The 2θ range was from 5 to 60° with a scanning speed of 2°/min and sample-to-detector distance of 185 mm.

Coin cells, of several configurations shown in Fig. 2a-c, were prepared in an argon-filled glove box to assess the electrochemical behavior of the composite films. Figure 2a depicts cells containing POEM-*b*-PBMA/VO_x/CB films as cathodes and a POEM-*b*-PBMA solid polymer electrolyte (SPE)[20] to enable a seamless interface. For these cells, polymer films (~30 μm) doped with $LiCF_3SO_3$ at a Li:EO ratio of 1:20 acting as the solid electrolyte were cast from anhydrous tetrahydrofuran on a lithium metal disk (VWR Scientific) used as the anode. After casting the electrolyte, the coated disk was vacuum dried for 40 min to remove residual solvent. Then a porous polypropylene washer (Celgard 2300, Celgard, Inc., Charlotte, NC) was placed on the Li disk to prevent edge shorting, and the POEM-*b*-PBMA/VO_x/CB cathode was placed on top. Stainless steel current collectors were used on both sides of the cells. Cells were also made with the POEM-*b*-PBMA/VO_x/CB cathode films using liquid electrolyte containing 1 M $LiPF_6$ in ethylene carbonate:dimethyl carbonate (Merck kGaA) 1:1 by mass with a Celgard 2300 disk as a separator to prevent shorting (shown in Fig. 2b).

Cells for controls were prepared using conventional composite cathodes made of sol-gel vanadium oxide, CB and poly(vinylidene fluoride) (PVDF, Kynar) as a binder as shown in Fig. 2c. Conventional composite cathodes were made by mixing the active battery material (vanadium oxide) with 10 wt % PVDF, and 5 wt % Super P CB. N-methylpyrrolidone (NMP) (Sigma Aldrich) was added in the mixture and was cast onto aluminum foil (VWR Scientific) and allowed to dry. Lower current rates were explored using a potentiostat (Solartron 1287, Solartron Analytical, Oak Ridge, TN) controlled by a PC running CorrWare (Scribner Associates, Inc., Southern Pines, NC). Cycle testing was conducted galvanostatically at 25°C with a Maccor series 4000 automated test system. Voltage limits were set at 3.5 and 2.5 V with varying discharge and charge rates.

In addition, the conductivity of POEM-*b*-PBMA/VO_x/CB nanocomposite films was measured by impedance spectroscopy using a frequency response analyzer (Solartron 1255, Solartron Analytical, Oak Ridge, TN), coupled to a potentiostat (Solartron 1287, Solartron Analytical, Oak Ridge, TN) and controlled by a PC running commercially available software (Zplot, Scribner Associates, Inc., Southern Pines, NC). The test fixture consisted of two blocking electrodes made of stainless steel and a Teflon washer of known diameter fixed the specimen area. The thickness of the sample was measured using a micrometer before and after the conductivity measurement to verify its consistency throughout the experiment.

Control films containing POEM-*b*-PBMA block copolymer and salt with addition of vanadium oxide only or CB only were also fabricated and dried under similar conditions. The redox behavior of the POEM-*b*-PBMA/VO_x/CB films was compared to these control films using cyclic voltammetry (CV) in a three-electrode cell. Films were cast on indium tin oxide-coated glass substrates for three-electrode cell measurements. The electrolyte consisted of 1 M

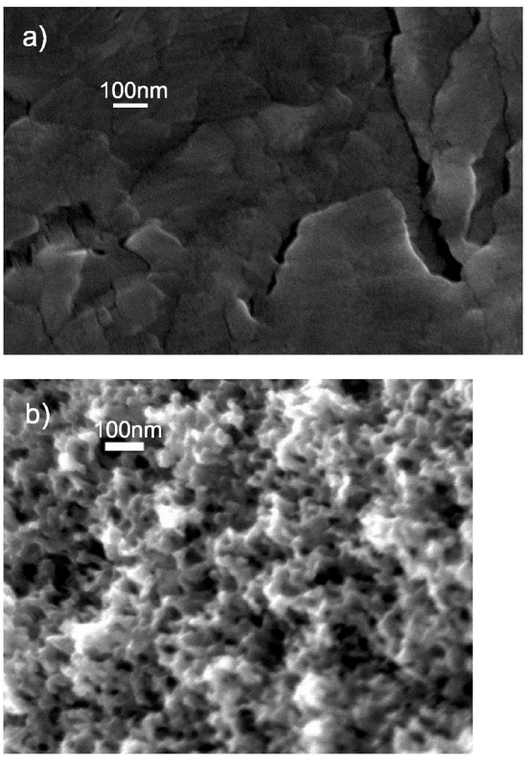

Figure 3. (a) SEM image of control film of vanadium oxide produced via sol-gel synthesis without polymer matrix and heated to 400°C. (b) SEM image of sol-gel vanadium oxide templated by POEM-*b*-PBMA, with polymer removed on heating to 400°C.

$LiClO_4$ in propylene carbonate. The reference electrode was a glass tube sealed at one end and containing a silver wire immersed in a solution of acetonitrile saturated with $AgNO_3$. A frit at the bottom of the tube enabled electrical contact with the electrolyte in the main chamber. A platinum foil served as the counter electrode. The potential was swept from 1.0 to 1.5 V vs Ag/Ag^+ at 50 mV/s using a potentiostat (Solartron 1287, Solartron Analytical, Oak Ridge, TN) controlled by a PC running CorrWare (Scribner Associates, Inc., Southern Pines, NC).

Results

As shown previously,[19] the microphase-separated morphology of POEM-*b*-PBMA serves to structure direct the growth of nanophase vanadium oxide within the ion-conducting POEM domains. On removing the polymer through pyrolysis, SEM could be used to better visualize the resulting oxide microstructure. Figure 3 shows the microstructure of the POEM-*b*-PBMA/VO_x films after pyrolysis at 400°C under argon (followed by a heating phase in air) along with that of a VO_x control (nontemplated) film heated under the same conditions. Elemental analysis performed on the templated film revealed that after the argon step of the pyrolysis 12 wt % carbon remained from the partial conversion of the copolymer and after the full heat-treatment ~0.13 wt % carbon remained. The microstructure of the control film (Fig. 3a) shows large featureless micron-sized plates. By contrast, the block copolymer-templated vanadium oxide (Fig. 3b) exhibits a high degree of porosity, with pore size and spacing that are consistent with the template morphology.[19] The surface area of the templated oxide was measured to be ~200 m^2/g using BET techniques, while the control had a surface area ~20 m^2/g.

The WAXS data shown in Fig. 4 verify that the orthorhombic

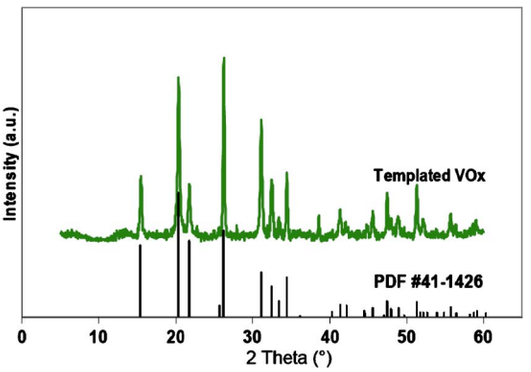

Figure 4. (Color online) WAXS pattern for sol-gel derived, block copolymer-templated vanadium oxide heated to 400°C.

structure of vanadium oxide is formed on heating to 400°C. The observed diffraction peaks match those of V_2O_5 (PDF no. 41-1426), shown below the experimental data.

Templated and control (nontemplated) vanadium oxide samples were mixed with PVDF, CB, and NMP, and cast on aluminum foil to create conventional composite cathodes. Cells were cycled with liquid electrolyte to assess the effects of the nanoporous oxide structure on cathode performance. Results of first discharge curves at C/10 and 10 C, where C/1 is defined as the current rate to discharge the theoretical capacity of V_2O_5 (147 mAh/g) in 1 *h*, from 2.5 to 3.5 V are shown in Fig. 5. The plateaus evident in the discharge profiles of both films are consistent with orthorhombic vanadium pentoxide.[4,14] At a rate of C/10, the capacities of the two cells are comparable, 150 mAh/g for the templated V_2O_5 vs 147 mAh/g for the control. Significantly, the first discharge capacity at 10 C for the templated cathode is 70% of the capacity at C/10, while the control at 10 C was only 27% of the C/10 capacity. The cycling data (which was reproduced in six different cells for each current rate) indicates a 2.5× improvement in capacity at 10 C for the templated cathodes. It is also noted that the capacities at 3 C for the templated and control samples were 96 and 58% of the C/10 capacity, respectively.

Cathodes were also prepared preserving the POEM-*b*-PBMA component to act as an electrolyte in all-solid-state cells. For these cells, films containing POEM-*b*-PBMA and V_2O_5 were cast with 5 wt % CB to wire the active material electronically. Prior to cast-

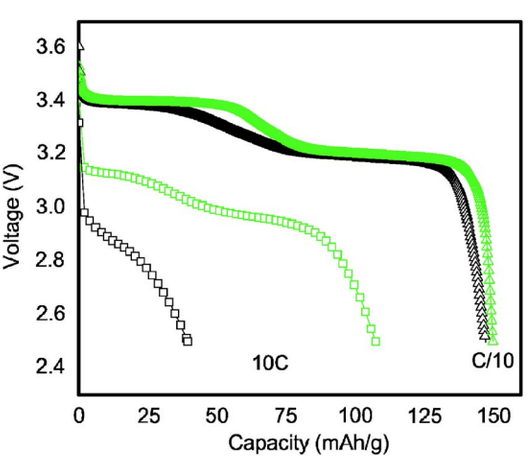

Figure 5. (Color online) Discharge profiles from crystalline composite cathodes made from templated and nontemplated sol-gel vanadium oxide. First discharge profiles are shown at C/10 (●) and 3C (□). The templated cathodes are shown in gray and the nontemplated are in black.

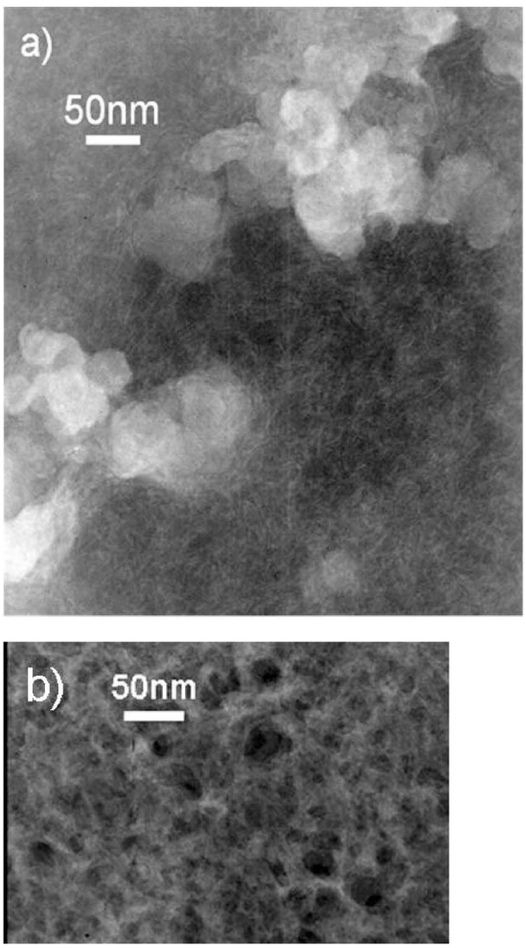

Figure 6. TEM micrographs of (a) POEM-*b*-PBMA containing 34 wt % V_2O_5 and 5 wt % CB and (b) POEM-*b*-PBMA/VO_x film without CB.

ing, the CB was treated with fuming sulfuric acid and a series of sonicating and cryogrinding steps to facilitate interaction with POEM chains and reduce particle aggregation. A TEM dark-field image depicting a cross section of the final POEM-*b*-PBMA/VO_x/CB nanocomposite film is shown in Fig. 6a. CB particles (acid-treated) are visible as light spherical regions (~40 nm diam). Also seen on careful inspection is the filamentous network structure of VO_x previously reported for POEM-*b*-PBMA/VO_x films;[19] dark portions of the image correspond to the PBMA domains. A TEM image of a POEM-*b*-PBMA/VO_x film without CB is shown in Fig. 6b for comparison. The filamentous structure of VO_x seen in Fig. 6b appears largely preserved in films containing CB, as exemplified in Fig. 6a. TEM revealed CB particles distributed throughout the films, although some aggregation of particles was observed.

Conductivity measurements on the films using impedance spectroscopy with blocking electrodes indicate a substantial improvement in conductivity in films with CB over those without. The conductivity of POEM-*b*-PBMA/VO_x films alone was $\sim 10^{-10}$ S/cm, while films with 5 wt % CB had values close to 10^{-5} S/cm. The conductivity was sufficient to allow use of the cathode films in an all-solid-state battery configuration.

POEM-*b*-PBMA/VO_x/CB films ~100 μm thick containing either acid-treated or untreated CB were used as cathodes in solid-state cells fitted with SPE (POEM-*b*-PBMA doped with $LiCF_3SO_3$ at 20:1 EO:Li) and lithium foil anodes. Representative cycling data at a C/10 rate for batteries employing cathodes prepared with acid-treated and untreated CB are shown in Fig. 7. The mass of the

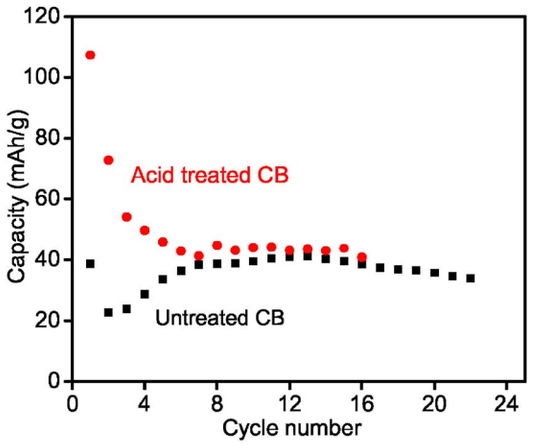

Figure 7. (Color online) Cycling data for solid-state batteries incorporating cathode films with untreated or acid-treated CB and with POEM-*b*-PBMA solid electrolyte.

electroactive phase in the cathode, the V_2O_5, was used to determine the capacity. The reversible capacity of the cell was ~40 mAh/g, and it cycled reversibly for over 20 cycles. The acid-treated CB sample shows an improved capacity compared to that of the untreated sample on the first and second cycles, but the capacity rapidly decays by the seventh cycle to around the same plateau value as that of the untreated sample. The increase in capacity with cycling seen for the untreated CB sample is similar to results reported previously for all-solid-state batteries incorporating microphase-separating electrolytes employing thin-film vanadium oxide cathodes.[20,22] In those studies, the improvement with cycling was hypothesized to be linked to the reorientation of the polymer electrolyte morphology under the applied potential.

To verify that the origin of the observed capacity was the intercalation of Li^+ into vanadium oxide, control films were tested by CV in a three-electrode configuration. Three voltammograms are depicted in Fig. 8a for films containing POEM-*b*-PBMA with VO_x, CB, or both. Blowups of the CV curves for the POEM-*b*-PBMA/VO_x and POEM-*b*-PBMA/CB composite films are shown in Fig. 8b. The vanadium oxide film alone is characterized by one set of corresponding redox peaks reflecting intercalation/deintercalation of Li^+ into/from the VO_x structure, while the POEM-*b*-PBMA/CB film mainly exhibits capacitive behavior. The POEM-*b*-PBMA/VO_x/CB film exhibits the same peaks, but the current obtained from this film is a factor of 20 higher.

Even though films cycled reversibly in solid-state batteries, their capacity was a great deal lower than that of the theoretical capacity for vanadium oxide of 147 mAh/g. To discover the origin of this disparity in capacity, cathodes were cycled with solid electrolyte of three different thicknesses, using cathode films incorporating acid-treated CB. In recognition of the decrease in capacity upon cycling, data are plotted from the second cycle. The test was repeated three times for each thickness to verify reproducibility. Representative curves for the second discharge step for these films, shown in Fig. 9, indicate no plateaus in voltage, as would be expected for an amorphous material. The total capacity for these films varied by ~5 to 10 mAh/g for each electrolyte thickness investigated; however, the trend of decreasing capacity with increasing solid electrolyte thickness was always observed. The second discharge capacities for ~30, 60, and 90 μm SPE films were 97, 63, and 22 mAh/g, respectively. These data indicate that one limit of the cell's capacity is the low ionic conductivity of the electrolyte. Reducing the thickness of the electrolyte, or employing an electrolyte of higher conductivity,[22] should result in a closer alignment of measured and theoretical values of capacity.

To investigate improvements in rate capability afforded by

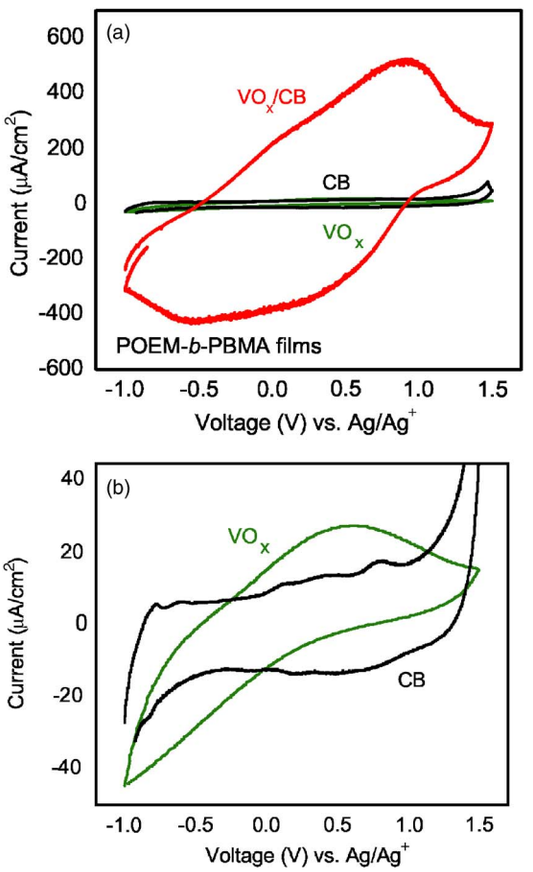

Figure 8. (Color online) Cyclic voltammograms for POEM-*b*-PBMA films containing (a) VO_x and/or CB on ITO in $LiClO_4$/propylene carbonate electrolyte and (b) only VO_x or CB. Swept from −1.0 to 1.5 V at 50 mV/s vs Ag/Ag^+.

the coassembly of vanadium oxide with POEM-*b*-PBMA, POEM-*b*-PBMA/VO_x/CB nanocomposite films were cycled with LP50 liquid electrolyte and compared to conventional composite cathode films. Data from these cycling experiments are shown in Fig. 10. The area and weight of active material were held constant

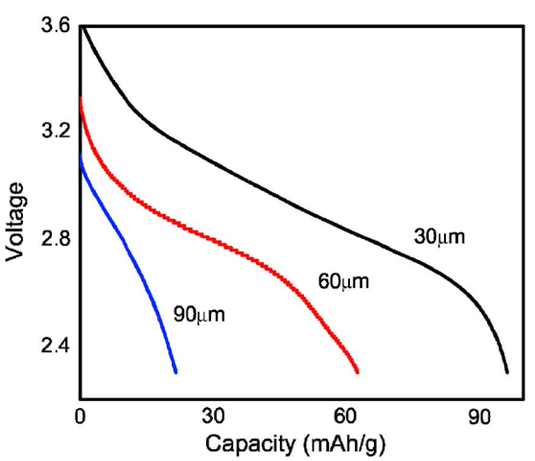

Figure 9. (Color online) Discharge profiles for the second cycle of three solid-state batteries using three different thicknesses of POEM-*b*-PBMA electrolyte as indicated.

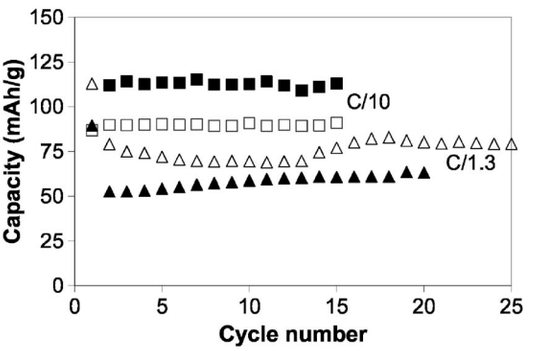

Figure 10. Cycling data for cells made with liquid electrolyte and using either nanostructured POEM-*b*-PBMA/VO_x/CB film cathode (open shapes) or control cathode (filled shapes).

for each of the cathodes cycled. The open shapes correspond to the nanocomposite cathode film while the filled shapes are for the control. The capacities of batteries employing liquid electrolyte (~90 mAh/g at C/10) was improved over those using the SPE (~40 mAh/g for the same rate). Although the conventional cathode begins with a higher capacity at the low charge/discharge rate of C/10, the nanocomposite film shows less capacity loss and higher capacity at the higher rate of C/1.3. At current rates of C/1.3, the nanostructured cathode maintains 85% of the capacity obtained at C/10, while the control maintains ~55% of that capacity. The cycling data indicate the ability to cycle these materials as cathodes in rechargeable lithium batteries and demonstrate a rate capability improvement for the nanocomposite cathode. The capacity/rate enhancements observed in this work are consistent with findings reported elsewhere on other active electrode materials coassembled into nanocomposite electrodes using structure-directing agents.[23-25]

Conclusion

Cathode films containing a nanoscale vanadium oxide phase were fabricated using POEM-*b*-PBMA as a structure-directing matrix and CB as a conductivity additive. The films were cycled in all-solid-state batteries using POEM-*b*-PBMA as the electrolyte to provide a seamless interface between cathode and electrolyte. The cell performance was found to be limited, however, by the low ionic conductivity of the electrolyte,[20] as demonstrated by the dependence of the capacity on polymer electrolyte thickness, and by the higher observed capacities in films cycled in the presence of a liquid electrolyte. The nanostructured morphology of the vanadium oxide gave improved rate performance over that of conventional cathode geometries.

A potential alternative to improving the electronic conductivity of the vanadium oxide would be the partial conversion of the polymer to graphitic carbon through heating after the sol-gel processing of vanadium oxide, resulting in carbon coating on the oxide surfaces. Odani et al. have produced carbon-coated vanadium oxide through their RAPET method (which stands for reaction under autogenic pressure at elevated temperatures) using a vanadyl alkoxide precursor.[26] Sides et al. have used similar carbonization strategies to improve the conductivity of $LiFePO_4$ by pyrolizing a polycarbonate template.[12] With vanadium oxide chemistries, unlike iron phosphate, there is a balance between preserving the graphitized carbon from pyrolyzed hydrocarbons in the system and avoiding reduction of the Li^+ insertion material V_2O_5 to less desirable oxides, such as VO_2 and V_2O_3. Investigating this approach to improve electronic conductivity could be the topic of future study.

Acknowledgments

This work was sponsored by the Office of Naval Research under contract no. N00014-05-1-0056 and, in part, by the MIT MRSEC Program of the National Science Foundation under award grant no.

DMR-0213282. This work made use of Shared Experimental Facilities under the MRSEC Program of the National Science Foundation under award grant no. DMR-0213282. The authors gratefully acknowledge Dr. Steve Kooi for his assistance with the BET work.

Massachusetts Institute of Technology assisted in meeting the publication costs of this article.

References

1. M. S. Whittingham, Y. Song, S. Lutta, P. Y. Zavalij, and N. A. Chernova, *J. Mater. Chem.*, **15**, 3362 (2005).
2. J. Livage, *Solid State Ionics*, **50**, 307 (1992).
3. F. Chaput, B. Dunn, P. Fuqua, and K. Salloux, *J. Non-Cryst. Solids*, **188**, 11 (1995).
4. G. Sudant, E. Baudrin, B. Dunn, and J. M. Tarascon, *J. Electrochem. Soc.*, **151**, A666 (2004).
5. J. H. Harreld, W. Dong, and B. Dunn, *MRS Bull.*, **33**, 561 (1998).
6. F. Coustier, J.-M. Lee, S. Passerini, and W. H. Smyrl, *Solid State Ionics*, **116**, 279 (1999).
7. F. Coustier, S. Passerini, and W. H. Smyrl, *J. Electrochem. Soc.*, **145**, L73 (1998).
8. E. Baudrin, G. Sudant, D. Larcher, B. Dunn, and J. M. Tarascon, *Chem. Mater.*, **18**, 4369 (2006).
9. H. Yamada, K. Tagawa, M. Komatsu, I. Moriguchi, and T. Kudo, *J. Phys. Chem. C*, **111**, 8397 (2007).
10. A. Singhal, G. Skandan, G. Amatucci, F. Badway, N. Ye, A. Manthiram, H. Ye, and J. J. Xu, *J. Power Sources*, **129**, 38 (2004).
11. C. J. Patrissi and C. R. Martin, *J. Electrochem. Soc.*, **146**, 3176 (1999).
12. C. J. Patrissi and C. R. Martin, *J. Electrochem. Soc.*, **148**, A1247 (2001).
13. C. R. Sides, F. Croce, V. Y. Young, C. R. Martin, and B. Scrosati, *Electrochem. Solid-State Lett.*, **8**, A484 (2005).
14. Y. Wang and G. Z. Cao, *Chem. Mater.*, **18**, 2787 (2006).
15. C. K. Chan, H. L. Peng, R. D. Twesten, K. Jarausch, X. F. Zhang, and Y. Cui, *Nano Lett.*, **7**, 490 (2007).
16. C. R. Sides and C. R. Martin, *Adv. Mater. (Weinheim, Ger.)*, **17**, 125 (2005).
17. M. E. Spahr, P. Stoschitzki-Bitterli, R. Nesper, O. Haas, and P. Novak, *J. Electrochem. Soc.*, **146**, 2780 (1999).
18. K. Takahashi, Y. Wang, and G. Cao, *Appl. Phys. Lett.*, **86**, 053102 (2005).
19. E. A. Olivetti, J. H. Kim, D. R. Sadoway, A. Asetakin, and A. M. Mayes, *Chem. Mater.*, **18**, 2828 (2006).
20. P. E. Trapa, B. Huang, Y.-Y. Won, D. R. Sadoway, and A. M. Mayes, *Electrochem. Solid-State Lett.*, **5**, A85 (2002).
21. H. Huang and L. F. Nazar, *Angew. Chem., Int. Ed.*, **40**, 3880 (2001).
22. P. E. Trapa, Y.-Y. Won, S. C. Mui, E. A. Olivetti, B. Huang, D. R. Sadoway, A. M. Mayes, and S. Dallek, *J. Electrochem. Soc.*, **152**, A1 (2005).
23. S. C. Mui, P. E. Trapa, B. Huang, P. P. Soo, M. I. Lozow, T. C. Wang, R. E. Cohen, A. N. Mansour, S. Mukerjee, A. M. Mayes, and D. R. Sadoway, *J. Electrochem. Soc.*, **149**, A1610 (2002).
24. S. Bullock and P. J. Kofinas, *J. Power Sources*, **132**, 256 (2004).
25. K. T. Nam, D. W. Kim, P. Yoo, C. Y. Chiang, N. Meethong, P. T. Hammond, Y. M. Chiang, and A. M. Belcher, *Science*, **312**, 885 (2006).
26. A. Odani, V. G. Pol, S. V. Pol, M. Koltypin, A. Gedanken, and D. Aurbach, *Adv. Mater. (Weinheim, Ger.)*, **18**, 1431 (2006).